HHS Public Access

Author manuscript

ACS Nano. Author manuscript; available in PMC 2021 June 23.

Published in final edited form as:

ACS Nano. 2020 June 23; 14(6): 6878–6886. doi:10.1021/acsnano.0c01007.

Targeted Delivery of Notch Inhibitor Attenuates Obesity-Induced Glucose Intolerance and Liver Fibrosis

Lauren R. Richter[○],
Departments of Pediatrics and Medicine, Columbia University, New York, New York 10032, United States

Qianfen Wan[○],
Pathology and Cell Biology, Columbia University, New York, New York 10032, United States

Di Wen[○],
Department of Bioengineering and California NanoSystems Institute, Jonsson Comprehensive Cancer Center and Center for Minimally Invasive Therapeutics, University of California, Los Angeles, California 90095, United States; Joint Department of Biomedical Engineering, University of North Carolina at Chapel Hill and North Carolina State University, Raleigh, North Carolina 27695, United States

Yuqi Zhang,
Department of Bioengineering, University of California, Los Angeles, California 90095, United States; Joint Department of Biomedical Engineering, University of North Carolina at Chapel Hill and North Carolina State University, Raleigh, North Carolina 27695, United States

Junjie Yu,
Medicine, Columbia University, New York, New York 10032, United States

Jin ku Kang,
Medicine, Columbia University, New York, New York 10032, United States

Changyu Zhu,
Department of Medicine, Columbia University, New York, New York 10032, United States; Department of Cancer Biology and Genetics, Sloan Kettering Institute, New York, New York 10065, United States

Elizabeth L. McKinnon,
Department of Pathology and Laboratory Medicine, University of British Columbia, Vancouver, British Columbia V6T 2B5, Canada

Zhen Gu,

Corresponding Authors: guzhen@g.ucla.edu, lq2123@columbia.edu, up2104@columbia.edu.
[○]L.R.R., Q.W., and D.W. contributed equally.

The authors declare the following competing financial interest(s): The authors have applied for a patent for GSI NPs.

ASSOCIATED CONTENT

Supporting Information

The Supporting Information is available free of charge at https://pubs.acs.org/doi/10.1021/acsnano.0c01007.

Serum lipids, liver lipids, transaminases, and comparison of hair graying between unencapsulated GSI and GSI NPs (Figures S1–S3) (PDF)

Complete contact information is available at: https://pubs.acs.org/10.1021/acsnano.0c01007

Department of Bioengineering and California NanoSystems Institute, Jonsson Comprehensive Cancer Center and Center for Minimally Invasive Therapeutics, University of California, Los Angeles, California 90095, United States; Joint Department of Biomedical Engineering, University of North Carolina at Chapel Hill and North Carolina State University, Raleigh, North Carolina 27695, United States

Li Qiang,
Pathology and Cell Biology, Columbia University, New York, New York 10032, United States

Utpal B. Pajvani
Medicine, Columbia University, New York, New York 10032, United States

Abstract

As the prevalence of obesity-induced type 2 diabetes mellitus (T2DM) and nonalcoholic steatohepatitis (NASH) continue to increase, the need for pharmacologic therapies becomes urgent. However, endeavors to identify and develop novel therapeutic strategies for these chronic conditions are balanced by the need for safety, impeding clinical translation. One shared pathology of these two diseases is a maladaptive reactivation of the Notch signaling pathway in liver. Notch antagonism with γ-secretase inhibitors effectively suppresses hepatic glucose production and reduces liver fibrosis in NASH, but its extrahepatic side effects, particularly goblet cell metaplasia, limit therapeutic utility. To overcome this barrier, we developed a nanoparticle-mediated delivery system to target γ-secretase inhibitor to liver (GSI NPs). GSI NP application reduced hepatic glucose production in diet-induced obese mice and reduced hepatic fibrosis and inflammation in mice fed a NASH-provoking diet, without apparent gastrointestinal toxicity. By changing the delivery method, these results provide proof-of-concept for the repurposing of a previously intolerable medication to address unmet needs in the clinical landscape for obesity-induced T2DM and NASH.

Keywords

drug delivery; nanomedicine; Notch inhibitor; nonalcoholic steatohepatitis; obesity; liver fibrosis

With the rise of obesity worldwide, the prevalence of comorbidities such as type 2 diabetes mellitus (T2DM), nonalcoholic fatty liver disease (NAFLD), and nonalcoholic steatohepatitis (NASH) are also increasing at alarming rates.[1–3] While the mechanisms by which obesity leads to its metabolic complications are still being investigated, the resulting demand for therapeutic interventions continues to be largely unmet. Despite numerous new pharmacologic entries to the market, T2DM remains the most common cause of end-stage renal disease and blindness in the United States and a major contributor to mortality.[4–6] Patients with NASH have even fewer options—without FDA-approved pharmacotherapy, the only effective treatment is liver transplantation.[7–9]

In obesity, excess lipid accumulation contributes to insulin resistance, which manifests in the liver as increased forkhead box protein O1 (Foxo1)-dependent hepatic glucose production (HGP).[10–12] In the absence of insulin, unphosphorylated Foxo1 binds to the insulin response element to promote transcription of glucose-6-phosphatase (G6PC) and

phosphoenolpyruvate carboxykinase (PCK1),[13] encoding the rate-limiting enzymes in glycogenolysis and gluconeogenesis, respectively.[14] Upon insulin presence and activation of PI3K/AKT, Foxo1 is phosphorylated and excluded from the nucleus, reducing HGP.[15] This signaling is disrupted in the insulin-resistant state, where Foxo1 is constitutively active.[16]

In investigating the effects of Foxo1 on T2DM pathophysiology, we uncovered a "re-activation" of the Notch signaling pathway in hepatocytes.[10] Notch is an evolutionarily conserved cell signaling system that directs embryonic development. Ligand binding induces γ-secretase-mediated Notch receptor cleavage, releasing the Notch intracellular domain (NICD). NICD translocates into the nucleus where it binds to mastermind-like protein 1 (MAML1) and the principle Notch effector, recombining the binding protein suppressor of hairless RBP-JK.[17–19] This complex promotes transcription of canonical Notch target genes, including the basic Helix–loop–helix (bHLH) hairy and enhancer of split (HES) and hairy/enhancer-of-split related with YRPW motif-like protein (HEYL) gene families,[19] that direct cell-fate decisions. In liver development, increased hepatoblast Notch activity directs differentiation into cholangiocytes and formation of bile ducts, with repression in adjacent cells leading to a hepatocyte lineage specification. Quiescent hepatocyte Notch activity persists into adulthood under typical physiologic conditions.[20] However, in obese mice and patients, we observed aberrant hepatocyte Notch activity that associated with the presence of T2DM as well as biochemical (plasma transaminase) and histological (NAFLD activity score) readouts of NASH.[21] Consistently, hepatocyte-specific Notch loss-of-function mice show attenuated diet-induced liver pathology, including improved glucose intolerance in mice fed an obesogenic high-fat diet (HFD), as well as reduced liver fibrosis in mice fed a novel NASH-provoking diet, whereas forced hepatocyte Notch activity accelerated diet effects in both models.[22,23]

These data suggested that pharmacologic Notch inhibitors would have metabolic benefits. The best studied Notch antagonists are small molecule inhibitors of the γ-secretase complex (GSI) that prevent activating cleavage of Notch receptors and are in clinical trials for cancer.[24–26] Indeed, GSI treatment reduced liver Notch activity, improved glucose metabolism, and ameliorated NASH diet-induced liver fibrosis but simultaneously caused goblet cell metaplasia related to intestinal Notch inhibition.[10,23,27,28] Based on these data, we hypothesized that liver-specific GSI administration may avoid intestinal side effects while retaining therapeutic potency. Nanomedicine-mediated treatment allows for enhanced targeted drug delivery, and many nanoparticle compositions, *i.e.*, poly(lactic coglycolic acid) (PLGA), have favorable biodegradability and biocompatibility profiles.[29,30] To test this potential, we developed PLGA-encapsulated GSI nanoparticles (GSI NPs) (Figure 1). Herein, we demonstrate that GSI NPs provide localized and effective inhibition of hepatic Notch signaling, improving obesity-induced glucose tolerance and liver fibrosis without apparent intestinal side effects.

RESULTS AND DISCUSSION

Synthesis and Characterization of GSI NPs

GSI NPs were prepared using an emulsion/solvent evaporation method to encapsulate dibenzazepine (a bioavailable γ-secretase inhibitor) in a PLGA matrix.[31] Dibenzazepine and

PLGA were dissolved in a dichloromethane (DCM) and 3% poly(vinyl alcohol) (PVA) solution. Empty (control) NPs were prepared using the same method without drug. The PLGA mixture was sonicated and dispersed into a 0.3% PVA solution, and the DCM was evaporated. The synthesized NPs, labeled with a Cy5.5 fluorophore, were collected by centrifuge. Resultant spherical NPs were ~180 nm in diameter as determined by dynamic light scattering, and their size remained relatively constant over 7 days (Figure 2a–d).

GSI NPs had a loading capacity of 8.9 ± 0.01% and an encapsulation efficiency of 88.6 ± 0.1%. To monitor the dissociation behavior and release kinetics of GSI, the NPs were loaded with 24 μg of GSI and incubated in phosphate-buffered solution (PBS) (pH 7.4) containing 20% ethanol at 37 °C. The NPs gradually disassociated due to the biodegradation of PLGA, triggering the encapsulated cargo release. This dissociation and sustained release occurred over 8 days as measured by the concentration of GSI in the buffer. In vivo, at 1 and 24 h after intravenous (IV) tail vein injection, nanoparticles were distributed primarily in the liver and kidneys, reflective of accumulation in the liver and renal excretion (Figure 2e).[32–34]

GSI NPs Block Liver Notch Activity

To assess Notch inhibition efficacy *in vivo*, we administered a single dose (5 μmol/kg, ~2.5 mg/kg) of GSI NPs suspended in normal saline to C57BJ/6 male mice by tail vein. GSI NPs were directly visualized in the liver (Figure 3a–c) but not the GI tract (Figure 3d). We next analyzed hepatic expression of Notch target genes—chosen empirically as targets that track with hepatocyte Notch activity *in vitro* and *in vivo*[35]—at multiple time points post-treatment and noted reduced liver Notch target gene expression at 2 and 4 days (Figure 3e).

GSI NPs Reverse Diet-Induced Glucose Intolerance

We next applied GSI NPs to a mouse model of diet-induced obesity (DIO) and glucose intolerance/insulin resistance. Eight-week-old C57BL/6 male mice were fed HFD (60% kcal from fat) for a total of 18 weeks (Figure 4a). After 14 weeks of diet-feeding, animals were randomized into two groups of equal body weight. We administered GSI or vehicle (control) NPs suspended in PBS by tail vein twice weekly for 4 weeks. GSI NP-treated mice showed significant improvements in glucose tolerance after a 2 g/kg glucose load as compared to control NP-treated mice (Figure 4b,c). Consistently, we observed reduced fasting glucose levels in GSI NP-treated mice (Figure 4d), despite similar body fat as measured by magnetic resonance imaging (MRI), commensurate with unchanged body, liver, inguinal white adipose tissue (iWAT), and epididymal white adipose tissue (eWAT) weights (Figure 4e–g). We observed no significant differences in liver lipid content or transaminases (aspartate transaminase [AST] and alanine transaminase [ALT]) and only trivial differences in serum lipids (Figure S1). These data suggest that GSI NP treatment improves glucose tolerance but not due to alterations in body weight, adiposity, or liver lipid content/injury.

We next assessed potential molecular pathways for improved glucose tolerance in GSI NP-treated mice. As expected, GSI NPs reduced Notch target gene expression by ~34–58%. We also observed a significant reduction in *Foxo1* expression, leading to reduction in multiple Foxo1 target genes including those associated with hepatic glucose production (Figure 4h).[36] Western blots similarly demonstrated a significant ~38% decrease in liver Foxo1 in GSI

NP-treated mice, with a proportional reduction in phosphorylated Foxo1 but unchanged phosphorylated Akt (Figure 4i). Taken together, these data suggest that GSI NP-induced amelioration of obesity-induced glucose tolerance is due to reduced Foxo1-mediated HGP.

GSI NPs Treatment Does Not Cause GI or Splenic Toxicity

We observed mild hair graying in 80% of GSI NP-treated mice, although subjectively less than in mice injected with unencapsulated GSI (Figure S2), which has been previously described.[37] Hair graying has also been noted in clinical trials of oral GSI for Alzheimer's Disease,[38,39] suggestive of dermal distribution of GSI regardless of method of administration. We next investigated two other known GSI side effects: intestinal metaplasia and marginal zone atrophy in the spleen.[26,40] We visualized minimal Cy5.5 signal in the small intestine of both control and GSI NP-treated mice; consistently, the goblet cell number was unchanged in the GSI NP-treated group (Figure 5a). This is in sharp contrast to mice treated with unencapsulated GSI at a similar dose, which shows a 3-fold increase in goblet cells,[23] leading to mucinous diarrhea, dehydration, weight loss, and eventually death.[41]

As anticipated based on NP size, we observed Cy5.5 signal in the spleen but no other extrahepatic tissues, indicating the presence of the NP shell (Figure 5b).[32,33] Though drug concentration was not directly measured, we observed unchanged splenic Notch activity—as assessed by expression of the most highly abundant *Hes/Hey* genes in spleen (*Hes1*, *Hes6*)—in GSI NP-treated animals (Figure 5c). Consistently, our pathologist did not detect differences in splenic architecture in representative samples analyzed in a blinded fashion (Figure 5d). We conclude that the Cy5.5 signal in the spleen may represent NP shells scavenged by circulating monocytes or accumulative entrapment of a small percentage of NPs over time, as the spleen did not demonstrate significant signal in the initial 24 h after injection (Figure 2e). Together, these data suggest that while GSI NPs may circulate to other organs through systemic circulation, the majority of drug action occurs in the liver as intended.

GSI NPs Reverse NASH-Induced Liver Fibrosis without GI Toxicity

We have observed aberrant hepatocyte Notch activity in patients with NASH or mice fed a NASH-provoking diet enriched in fructose, palmitate, and cholesterol with *ad libitum* access to fructose-containing drinking water.[21] Systemic GSI treatment reduces liver fibrosis in these mice, but with significant GI toxicity.[23] To test the safety and efficacy of GSI NPs to ameliorate NASH-induced liver fibrosis, we applied GSI or vehicle (control) NPs twice weekly for 4 weeks to weight-matched, NASH diet-fed C57BL/6 male mice (Figure 6a).[22,23] We observed no differences in body weight, body composition, or tissue weights between groups (Figure 6b–f). Further, and consistent with phenotypes from hepatocyte-specific Notch loss-of-function mice and GSI NP-treated HFD-fed mice, we observed trivial changes in serum or liver lipids and serum transaminases (Figure S3).[23] Nevertheless, GSI NPs reduced Notch target gene expression with a parallel and significant reduction in inflammatory and fibrogenic gene expression (Figure 6g).[42] Consistently, we observed a 32% reduction in liver collagen staining (Figure 6h) and a 27% reduction in liver macrophage number (Figure 6i), which contribute to both liver inflammation and fibrosis.[43,44] All GSI NP-treated animals had mild hair graying but showed no increase in intestinal

goblet cell number as compared to control (not shown and Figure 6j). Overall, these data suggest that GSI NPs can ameliorate NASH diet-induced liver fibrosis and inflammation without the intestinal toxicity of unencapsulated GSI treatment.

CONCLUSIONS

We described a drug delivery technique based on liver PLGA NP uptake to block pathologic hepatocyte Notch signaling while reducing the toxic profile of traditional GSI administration. GSI NPs reduced HFD-induced glucose intolerance as well as hepatic fibrosis and inflammation in a dietary NASH mouse model. These encouraging effects are consistent with systemic Notch signaling inhibition but circumvent intestinal and splenic toxicity. Though serum concentrations of GSI were not compared directly in this study, the comparable efficacy in metabolic end points from previous work suggests that NP administration delivers therapeutic doses of GSI to intended targets while reducing or avoiding toxicity in other tissues. These data provide proof-of-concept that nanomedicine allows for repurposing of a previously intolerable medication and lay the groundwork for future investigations focusing on sustained drug effect and the potential reversibility of NASH fibrosis, addressing unmet needs in the clinical landscape for obesity.

METHODS

Preparation of Dibenzazepine-Loaded Nanoparticles

PLGA nanoparticles were prepared with an emulsion/solvent evaporation method. Briefly, 1 mg of dibenzazepine (Selleck Chemicals, S2711 or Syncom, 209984–56-5) and 10 mg of PLGA (Sigma) were dissolved in 0.8 mL of DCM, followed by the addition of 2 mL of 0.3% PVA solution. This mixture was then sonicated using a probe sonicator (amplitude 30, 15 s on, 15 s off × 10 min) and dispersed into 8 mL of 0.3% PVA solution under stirring. Finally, DCM was evaporated using a rotary evaporator. GSI NPs were labeled by adding 0.5% Cy5.5 fluorophore and PLGA (w/w) while dissolving the dibenzazepine and PLGA. Empty (control) NPs were fabricated using the same method without drug. The synthesized NPs were collected by centrifuge at 13000 rpm for 45 min. Resultant NPs were spherical in shape and ~180 nm in diameter. NPs were then analyzed for loading capacity (LC) and encapsulation efficiency (EE). LC and EE of GSI were determined by high-performance liquid chromatography (HPLC) using an Agilent C18 column (4.6 × 50 mm) eluted with water and acetonitrile (starting at 95:5 and then after 6 min, gradient up to 5:95; wavelength 254 nm). LC and EE were calculated as LC = B/C × 100% and EE = B/A × 100%, where A equals the expected encapsulated amount of GSI using a standard curve, B equals the encapsulated amount of GSI, and C equals the total weight of the particles. Particle size and polydispersity intensity were measured by dynamic light scattering. The zeta potential of the NPs was determined by their electrophoretic mobility after dilution in DI water using the same instrument. NP morphology was assessed by a FEI Verios 460L field-emission scanning electron microscope.

In Vitro Release Studies

The *in vitro* release profile of GSI-loaded PLGA nanoparticles was evaluated through incubation of NPs in 25 mL PBS buffer (NaCl, 137 mM; KCl, 2.7 mM; Na_2HPO_4, 10 mM; KH_2PO_4, 2 mM; pH 7.4) containing 20% ethanol at 37 °C on an orbital shaker (100 rpm/min). At predetermined time points, the buffer sample was taken for HPLC analysis (C18 reversed-phase column 4.6 mm × 15 cm, wavelength: 254 nm) of GSI with the mobile phase composed of water and acetonitrile (starting at 95:5, then after 6 min, gradient up to 5:95, then back to 95:5 in 2 min, $n = 3$).

Animals

Unless otherwise specified, seven-week old male C57BL/6 mice were obtained from Jackson Laboratories (Bar Harbor, ME). All animals were treated in accordance with the Guide for Care and Use of Laboratory Animals, and protocols were approved by the Columbia Institutional Animal Care and Use Committee (IACUC). Mice were caged at 22 ± 1 °C with free access to water and diet on a 12 h light/dark cycle unless otherwise specified. Mice were adapted to their environment for at least 1 week prior to starting experiments.

In Vivo Studies

Male C57BL/6 were fed either normal chow diet (Purina Mills 5053), a high-fat diet (60% kcal from fat, Research Diets D12492), or a NASH-provoking diet (Envigo Teklad Diets TD.160785) with *ad libidum* access to sucrose–fructose-containing drinking water (MilliporeSigma D-(–)-fructose F0127 and sucrose S0389). Four weeks prior to sacrifice, animals were randomized to control or GSI NPs (5 μmol/kg, ~2.5 mg/kg) injected twice weekly (q 3–4 days) by tail vein injection. The HFD-fed group received a total of nine doses over the course of the experiment (45 μmol/kg, ~22.5 mg/kg), and the NASH diet-fed group received eight doses total (40 μmol/kg, ~20 mg/kg). MRI was performed immediately prior to the final injection. At sacrifice, animals were euthanized by CO_2 inhalation followed by cervical dislocation, and blood, liver, kidney, spleen, heart, and adipose tissues (iWAT and eWAT) were collected for analyses. Blood samples coagulated for 15 min prior to collecting serum.

IP Glucose Tolerance Tests

After eight NP treatments, mice were fasted for 16 h (overnight) before intraperitoneal injection of 2 g/kg glucose solution. Blood glucose levels were monitored every 30 min for 120 min by tail vein (Bayer Contour glucose meter).

Visualization of NPs

Snap-frozen liver, kidney, heart, and intestine sections were fixed with 4% paraformaldehyde at 4 °C for 48 h prior to dehydration with 30% sucrose solution for 72 h at room temperature. Frozen tissue specimens were embedded in optimal cutting temperature (OCT) cutting media (Sakura Tissue-Tek O.C.T. Compound 4583) and mounted in 5 μm thickness sections. Direct visualization of Cy5.5 signal from the nanoparticles was performed using fluorescent microscopy and quantified over background (as measured by tissue fluorescence

from noninjected animals, $n = 4$). Representative images were taken using a Zeiss light microscope coupled with an AxioCam MR3 camera (Carl Zeiss).

Serum Assays

Serum triglycerides and cholesterol were measured according to the manufacturer's instructions using colorimetric assays (Thermo Fisher Scientific [TFS] Infinity Cholesterol Liquid Stable Reagent TR13421 and Infinity Triglycerides Liquid Stable Reagent TR22421). Serum AST (TFS Infinity AST [GOT] Liquid Stable Reagent TR70121) and ALT (Teco Diagnostics ALT [SGPT] Liquid Reagent [Kinetic Method] A524–150) were measured per the manufacturer's instructions using standard colorimetric or kinetic assays. Serum insulin levels were measured per manufacturer's instructions using a Mercodia Mouse Insulin ELISA kit (10–1247-01).

Liver Lipid Measurements

Liver lipids were extracted using the Folch method.[45] In brief, ~100 mg of snap frozen liver tissue was homogenized in 1× PBS. Sample was added to a chloroform–methanol mixture and the aqueous layer evaporated under N_2 gas. Lipid content was measured with colorimetric assays as above.

Quantitative Reverse-Transcription PCR

RNA was extracted from liver and spleen with Trizol (Invitrogen) prior to cDNA synthesis (Applied Biosystems) and quantitative PCR with a DNA Engine Opticon 2 System (Bio-Rad) and GoTaq qPCR Master Mix (Promega A600A). mRNA levels were normalized to *Rpl23* mRNA using the ΔΔC(t) method and are presented as relative transcript levels to control. Primer sequences are available upon request.

Histological Assessments

Paraffin-fixed sections of the spleen were fixed with 10% formaldehyde for 48 h and stored in 70% ethanol for 72 h at room temperature prior to mounting in 5 μm thickness sections and hematoxylin and eosin staining. Images of the entire specimen were sent to a blinded pathologist (ELM) and examined based on the presence or absence of marginal zone atrophy. Paraffin-fixed sections of the liver were fixed with 10% formaldehyde for 48 h and stored in 70% ethanol for 72 h at room temperature prior to mounting in 5 μm thickness sections. For each liver, 12–18 images of nonoverlapping Picrosirius Red-stained regions were used to quantify collagen deposition under polarized light microscopy (Olympus IX 70) using ImageJ (NIH) software as previously described.[46,47] Snap frozen liver sections were fixed with 4% paraformaldehyde at 4 °C for 48 h prior to dehydration with 30% sucrose solution for 72 h at room temperature. Specimens were then embedded in OCT compound and mounted in 5 μm thickness sections. For each liver, 12–18 images of nonoverlapping F4/80-stained (Cell Signaling Technology [CST] #70076, 1:500 dilution) regions were examined under brightfield microscopy (Olympus IX 70) and analyzed by ImageJ (NIH) software as previously described using thresholding and area measurement.[46,47] Paraffin-fixed sections of small intestine were fixed with 10% formaldehyde for 48 h and stored in 70% ethanol solution for 72 h at room temperature. Periodic acid-Schiff (PAS)

stained sections of intestine were examined under brightfield microscopy (Olympus IX 70), and goblet cell numbers were quantified using ImageJ (NIH) software as previously described.[45]

Western Blots

Snap frozen liver tissue was lysed in a Triton-based lysis buffer to obtain whole-cell lysate. Protein was loaded on a 10% SDS–PAGE gel. Immunoblots were conducted on seven randomly chosen samples per group and incubated with primary antibodies (1:1000 dilution unless otherwise specified) against Akt (CST #9272), p-Akt^{T308} (CST #4056), Foxo1 (CST #2880), p-Foxo1^{S256} (CST #84192), and GAPDH (Proteintech HRP-60004, 1:5000 dilution). Quantification of signal was performed using ImageJ software as described.[46]

Statistical Analysis

Differences between groups were analyzed using a two-tailed unpaired Student's *t*-test assuming unequal variance with p-value <0.05 to determine significance. All results are presented as mean ± standard error of the mean (SEM). Statistical analysis was performed using Prism software (GraphPad).

Supplementary Material

Refer to Web version on PubMed Central for supplementary material.

ACKNOWLEDGMENTS

This work was supported by NIH Grant Nos. R01DK103818 (U.B.P.), R01DK112943 (L.Q.), R01DK119767 (U.B.P), and T32DK065522 (P.I.: S.E. Oberfield, support to L.R.R.), the Russell Berrie Foundation (L.Q. and Q.W.), the Endocrine Fellows Foundation (L.R.R.), and the start-up package of UCLA (Z.G.). We acknowledge excellent technical support from T. Kolar and A. Flete at Columbia University.

REFERENCES

(1). Adams LA; Waters OR; Knuiman MW; Elliott RR; Olynyk JK NAFLD as a Risk Factor for the Development of Diabetes and the Metabolic Syndrome: An Eleven-Year Follow-Up Study. Am. J. Gastroenterol. 2009, 104, 861–867. [PubMed: 19293782]

(2). Hossain N; Afendy A; Stepanova M; Nader F; Srishord M; Rafiq N; Goodman Z; Younossi Z Independent Predictors of Fibrosis in Patients with Nonalcoholic Fatty Liver Disease. Clin. Gastroenterol. Hepatol. 2009, 7, 1224–1229. [PubMed: 19559819]

(3). Williams CD; Stengel J; Asike MI; Torres DM; Shaw J; Contreras M; Landt CL; Harrison SA Prevalence of Nonalcoholic Fatty Liver Disease and Nonalcoholic Steatohepatitis among a Largely Middle-Aged Population Utilizing Ultrasound and Liver Biopsy: A Prospective Study. Gastroenterology 2011, 140, 124–131. [PubMed: 20858492]

(4). Collins AJ; Foley RN; Chavers B; Gilbertson D; Herzog C; Johansen K; Kasiske B; Kutner N; Liu J; St Peter W; Guo H; Gustafson S; Heubner B; Lamb K; Li S; Li S; Peng Y; Qiu Y; Roberts T; Skeans M; et al. United States Renal Data System 2011 Annual Data Report: Atlas of Chronic Kidney Disease & End-Stage Renal Disease in the United States. Am. J. Kidney Dis. 2012, 59 (1), No. A7.

(5). Lee R; Wong TY; Sabanayagam C Epidemiology of Diabetic Retinopathy, Diabetic Macular Edema and Related Vision Loss. Eye Vis., London 2015, 2, 17.

(6). Murphy SL; Xu J; Kochanek KD; Curtin SC; Arias E Deaths: Final Data for 2015. Natl. Vital Stat. Rep. 2017, 66, 1–75.

(7). Oseini AM; Sanyal AJ Therapies in Non-Alcoholic Steatohepatitis (NASH). Liver Int. 2017, 37 (Suppl 1), 97–103. [PubMed: 28052626]

(8). Rinella ME Nonalcoholic Fatty Liver Disease: A Systematic Review. JAMA, J. Am. Med. Assoc. 2015, 313, 2263–2273.

(9). Gottlieb A; Mosthael W; Sowa JP; Canbay A Nonalcoholic-Fatty-Liver-Disease and Nonalcoholic Steatohepatitis: Successful Development of Pharmacological Treatment Will Depend on Translational Research. Digestion 2019, 100, 79–85. [PubMed: 30537758]

(10). Pajvani UB; Shawber CJ; Samuel VT; Birkenfeld AL; Shulman GI; Kitajewski J; Accili D Inhibition of Notch Signaling Ameliorates Insulin Resistance in a FoxO1-Dependent Manner. Nat. Med. 2011, 17, 961–967. [PubMed: 21804540]

(11). Petersen MC; Vatner DF; Shulman GI Regulation of Hepatic Glucose Metabolism in Health and Disease. Nat. Rev. Endocrinol. 2017, 13, 572–587. [PubMed: 28731034]

(12). Lin HV; Accili D Hormonal Regulation of Hepatic Glucose Production in Health and Disease. Cell Metab. 2011, 14, 9–19. [PubMed: 21723500]

(13). Haeusler RA; Kaestner KH; Accili D FoxOs Function Synergistically to Promote Glucose Production. J. Biol. Chem. 2010, 285, 35245–35248. [PubMed: 20880840]

(14). Nakae J; Biggs WH 3rd; Kitamura T; Cavenee WK; Wright CV; Arden KC; Accili D Regulation of Insulin Action and Pancreatic Beta-Cell Function by Mutated Alleles of the Gene Encoding Forkhead Transcription Factor Foxo1. Nat. Genet. 2002, 32, 245–253. [PubMed: 12219087]

(15). Nakae J; Park BC; Accili D Insulin Stimulates Phosphorylation of the Forkhead Transcription Factor FKHR on Serine 253 through a Wortmannin-Sensitive Pathway. J. Biol. Chem. 1999, 274, 15982–15985. [PubMed: 10347145]

(16). Altomonte J; Richter A; Harbaran S; Suriawinata J; Nakae J; Thung SN; Meseck M; Accili D; Dong H Inhibition of Foxo1 Function is Associated with Improved Fasting Glycemia in Diabetic Mice. Am. J. Physiol.: Endocrinol. Metab 2003, 285, E718–E728. [PubMed: 12783775]

(17). Wu L; Sun T; Kobayashi K; Gao P; Griffin JD Identification of a Family of Mastermind-Like Transcriptional Coactivators for Mammalian Notch Receptors. Mol. Cell. Biol. 2002, 22, 7688–7700. [PubMed: 12370315]

(18). Jarriault S; Brou C; Logeat F; Schroeter EH; Kopan R; Israel A Signalling Downstream of Activated Mammalian Notch. Nature 1995, 377, 355–358. [PubMed: 7566092]

(19). Kopan R; Ilagan MX The Canonical Notch Signaling Pathway: Unfolding the Activation Mechanism. Cell 2009, 137, 216–233. [PubMed: 19379690]

(20). Schwabe RF; Tabas I; Pajvani UB Mechanisms of Fibrosis Development in Nonalcoholic Steatohepatitis. Gastroenterology 2020, 158, 1913–1928.

(21). Valenti L; Mendoza RM; Rametta R; Maggioni M; Kitajewski C; Shawber CJ; Pajvani UB Hepatic Notch Signaling Correlates with Insulin Resistance and Nonalcoholic Fatty Liver Disease. Diabetes 2013, 62, 4052–4062. [PubMed: 23990360]

(22). Wang X; Zheng Z; Caviglia JM; Corey KE; Herfel TM; Cai B; Masia R; Chung RT; Lefkowitch JH; Schwabe RF; Tabas I Hepatocyte TAZ/WWTR1 Promotes Inflammation and Fibrosis in Nonalcoholic Steatohepatitis. Cell Metab. 2016, 24, 848–862. [PubMed: 28068223]

(23). Zhu C; Kim K; Wang X; Bartolome A; Salomao M; Dongiovanni P; Meroni M; Graham MJ; Yates KP; Diehl AM; Schwabe RF; Tabas I; Valenti L; Lavine JE; Pajvani UB Hepatocyte Notch Activation Induces Liver Fibrosis in Nonalcoholic Steatohepatitis. Sci. Transl. Med. 2018, 10, No. eaat0344.

(24). Takebe N; Nguyen D; Yang SX Targeting Notch Signaling Pathway in Cancer: Clinical Development Advances and Challenges. Pharmacol. Ther. 2014, 141, 140–149. [PubMed: 24076266]

(25). Plentz R; Park JS; Rhim AD; Abravanel D; Hezel AF; Sharma SV; Gurumurthy S; Deshpande V; Kenific C; Settleman J; Majumder PK; Stanger BZ; Bardeesy N Inhibition of Gamma-Secretase Activity Inhibits Tumor Progression in a Mouse Model of Pancreatic Ductal Adenocarcinoma. Gastroenterology 2009, 136, 1741–1749. [PubMed: 19208345]

(26). De Strooper B Aph-1, Pen-2, and Nicastrin with Presenilin Generate an Active Gamma-Secretase Complex. Neuron 2003, 38, 9–12. [PubMed: 12691659]

(27). van Es JH; van Gijn ME; Riccio O; van den Born M; Vooijs M; Begthel H; Cozijnsen M; Robine S; Winton DJ; Radtke F; Clevers H Notch/Gamma-Secretase Inhibition Turns Proliferative Cells in Intestinal Crypts and Adenomas into Goblet Cells. Nature 2005, 435, 959–963. [PubMed: 15959515]

(28). Sparling DP; Yu J; Kim K; Zhu C; Brachs S; Birkenfeld AL; Pajvani UB Adipocyte-Specific Blockade of Gamma- Secretase, but Not Inhibition of Notch Activity, Reduces Adipose Insulin Sensitivity. Mol. Metab. 2016, 5, 113–121. [PubMed: 26909319]

(29). Danhier F; Ansorena E; Silva JM; Coco R; Le Breton A; Preat V PLGA-Based Nanoparticles: An Overview of Biomedical Applications. J. Controlled Release 2012, 161, 505–522.

(30). Shive MS; Anderson JM Biodegradation and Biocompatibility of PLA and PLGA Microspheres. Adv. Drug Delivery Rev. 1997, 28, 5–24.

(31). Di J; Yao S; Ye Y; Cui Z; Yu J; Ghosh TK; Zhu Y; Gu Z Stretch-Triggered Drug Delivery from Wearable Elastomer Films Containing Therapeutic Depots. ACS Nano 2015, 9, 9407–9415. [PubMed: 26258579]

(32). Simon LC; Sabliov CM The Effect of Nanoparticle Properties, Detection Method, Delivery Route and Animal Model on Poly(Lactic-Co-Glycolic) Acid Nanoparticles Biodistribution in Mice and Rats. Drug Metab. Rev. 2014, 46, 128–141. [PubMed: 24303927]

(33). Mohammad AK; Reineke JJ Quantitative Detection of PLGA Nanoparticle Degradation in Tissues Following Intravenous Administration. Mol. Pharmaceutics 2013, 10, 2183–2189.

(34). Reineke J; Li M; Avgoustakis K Physiologically Based Pharmacokinetic Modeling of PLGA Nanoparticles with Varied mPEG Content. Int. J. Nanomed. 2012, 7, 1345–1356.

(35). Pajvani UB; Qiang L; Kangsamaksin T; Kitajewski J; Ginsberg HN; Accili D Inhibition of Notch Uncouples Akt Activation from Hepatic Lipid Accumulation by Decreasing mTorc1 Stability. Nat. Med. 2013, 19, 1054–1060. [PubMed: 23832089]

(36). Matsumoto M; Pocai A; Rossetti L; Depinho RA; Accili D Impaired Regulation of Hepatic Glucose Production in Mice Lacking the Forkhead Transcription Factor Foxo1 in Liver. Cell Metab. 2007, 6, 208–216. [PubMed: 17767907]

(37). Schouwey K; Beermann F The Notch Pathway: Hair Graying and Pigment Cell Homeostasis. Histol. Histopathol. 2008, 23, 609–619. [PubMed: 18283646]

(38). Doody RS; Raman R; Farlow M; Iwatsubo T; Vellas B; Joffe S; Kieburtz K; He F; Sun X; Thomas RG; Aisen PS; Alzheimer's Disease Cooperative Study Steering, C.; Siemers E; Sethuraman G; Mohs R; Semagacestat Study, G. A Phase 3 Trial of Semagacestat for Treatment of Alzheimer's Disease. N. Engl. J. Med. 2013, 369, 341–350. [PubMed: 23883379]

(39). Fleisher AS; Raman R; Siemers ER; Becerra L; Clark CM; Dean RA; Farlow MR; Galvin JE; Peskind ER; Quinn JF; Sherzai A; Sowell BB; Aisen PS; Thal LJ Phase 2 Safety Trial Targeting Amyloid Beta Production with a Gamma-Secretase Inhibitor in Alzheimer Disease. Arch. Neurol. 2008, 65, 1031–1038. [PubMed: 18695053]

(40). de Vera Mudry MC; Regenass-Lechner F; Ozmen L; Altmann B; Festag M; Singer T; Muller L; Jacobsen H; Flohr A Morphologic and Functional Effects of Gamma Secretase Inhibition on Splenic Marginal Zone B Cells. Int. J. Alzheimer's Dis. 2012, 2012, 289412. [PubMed: 23316412]

(41). Real PJ; Tosello V; Palomero T; Castillo M; Hernando E; de Stanchina E; Sulis ML; Barnes K; Sawai C; Homminga I; Meijerink J; Aifantis I; Basso G; Cordon-Cardo C; Ai W; Ferrando A Gamma-Secretase Inhibitors Reverse Glucocorticoid Resistance in T Cell Acute Lymphoblastic Leukemia. Nat. Med. 2009, 15, 50–58. [PubMed: 19098907]

(42). Tsuchida T; Friedman SL Mechanisms of Hepatic Stellate Cell Activation. Nat. Rev. Gastroenterol. Hepatol. 2017, 14, 397–411. [PubMed: 28487545]

(43). Pradere JP; Kluwe J; De Minicis S; Jiao JJ; Gwak GY; Dapito DH; Jang MK; Guenther ND; Mederacke I; Friedman R; Dragomir AC; Aloman C; Schwabe RF Hepatic Macrophages but Not Dendritic Cells Contribute to Liver Fibrosis by Promoting the Survival of Activated Hepatic Stellate Cells in Mice. Hepatology 2013, 58, 1461–1473. [PubMed: 23553591]

(44). Seki E; de Minicis S; Inokuchi S; Taura K; Miyai K; van Rooijen N; Schwabe RF; Brenner DA CCR2 Promotes Hepatic Fibrosis in Mice. Hepatology 2009, 50, 185–197. [PubMed: 19441102]

(45). Folch J; Lees M; Sloane Stanley GH A Simple Method for the Isolation and Purification of Total Lipides from Animal Tissues. J. Biol. Chem. 1957, 226, 497–509. [PubMed: 13428781]

(46). Schneider CA; Rasband WS; Eliceiri KW NIH Image to ImageJ: 25 Years of Image Analysis. Nat. Methods 2012, 9, 671–675. [PubMed: 22930834]

(47). Puchtler H; Waldrop FS; Valentine LS Polarization Microscopic Studies of Connective Tissue Stained with Picro-Sirius Red FBA. Beitr. Pathol. 1973, 150, 174–187. [PubMed: 4129194]

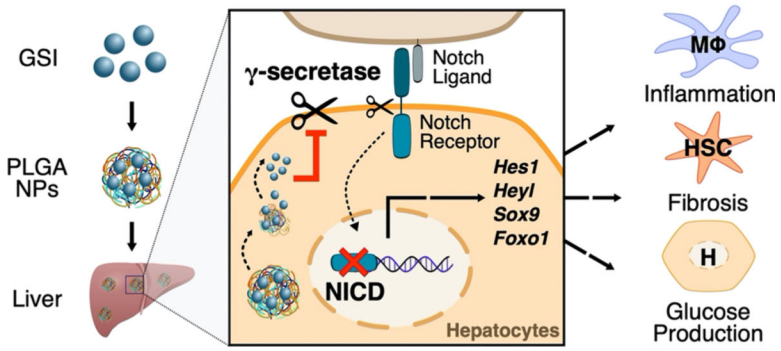

Figure 1.

Schematic of PLGA-encapsulated GSI Nanoparticles in the liver. GSI NPs accumulate in the liver, where they release GSI over time. Inhibition of γ-secretase prevents translocation of the Notch intracellular domain (NICD) into the nucleus, blocking target gene transcription. Downstream effects of Notch signaling inhibition include reduced macrophage (MΦ)-mediated inflammation, hepatic stellate cell (HSC)-induced fibrosis, and hepatocyte (H) glucose production.

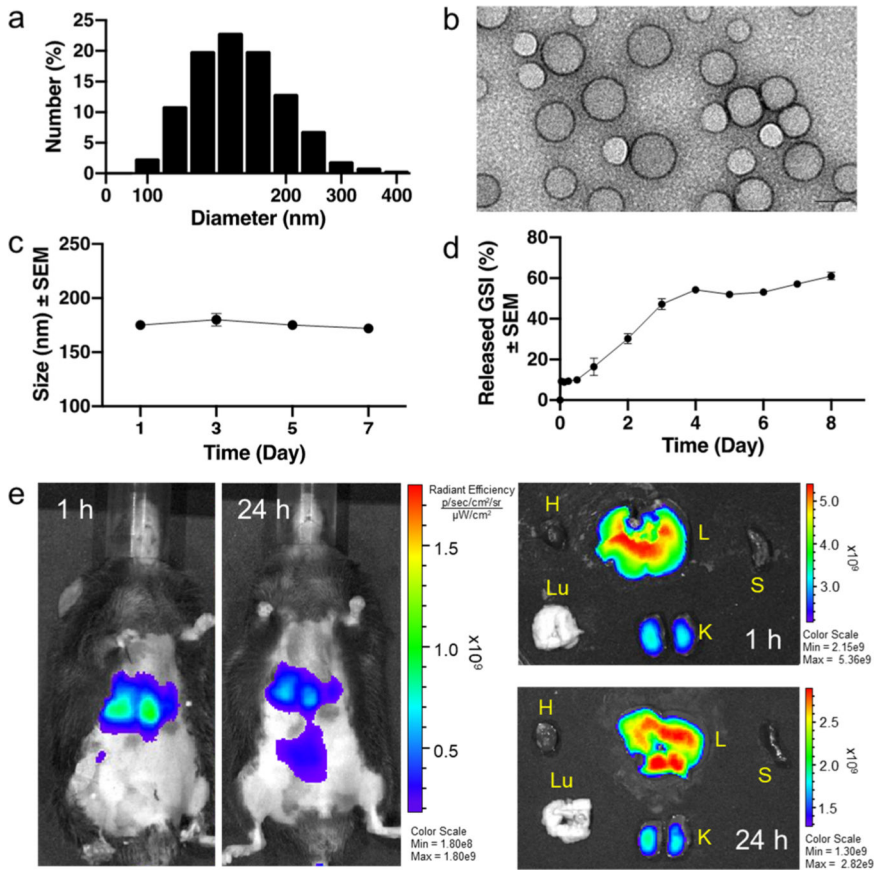

Figure 2.

GSI NP characteristics and biodistribution. (a) NP size distribution and (b) shape by scanning electron microscopy (scale bar: 0.1 μm). (c) Hydrodynamic nanoparticle size remained stable over 1 week. (d) Dissociation of nanoparticles measured by GSI concentration over time. (e) PLGA nanoparticles were distributed mainly in the liver (L) and kidneys (K) at 1 and 24 h post-tail vein injection, indicated by fluorescent signal. Other tissues, *e.g.*, heart (H), lungs (Lu), and spleen (S), did not show significant nanoparticle accumulation at 24 h. $n = 3$.

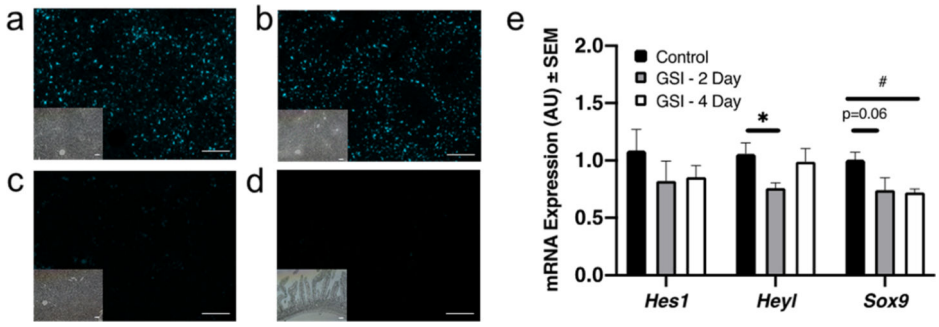

Figure 3.

GSI NPs reduces liver Notch activity. (a–d) Abundant liver Cy5.5 signal in (a) control- and (b) GSI NP-treated mice 4 days post injection (1 s exposure), as compared to (c) liver sections from an untreated animal (1 s exposure), or (d) small intestine from GSI NP-treated mice (5 s exposure). Bright field images provided for visualization of tissue architecture (scale bars = 200 μm). (e) Liver Notch target gene expression after a single GSI NP IV injection. *$p < 0.05$ for control *vs* GSI 2 day. #$p < 0.05$ for control *vs* GSI 4 day, $n = 5$/group.

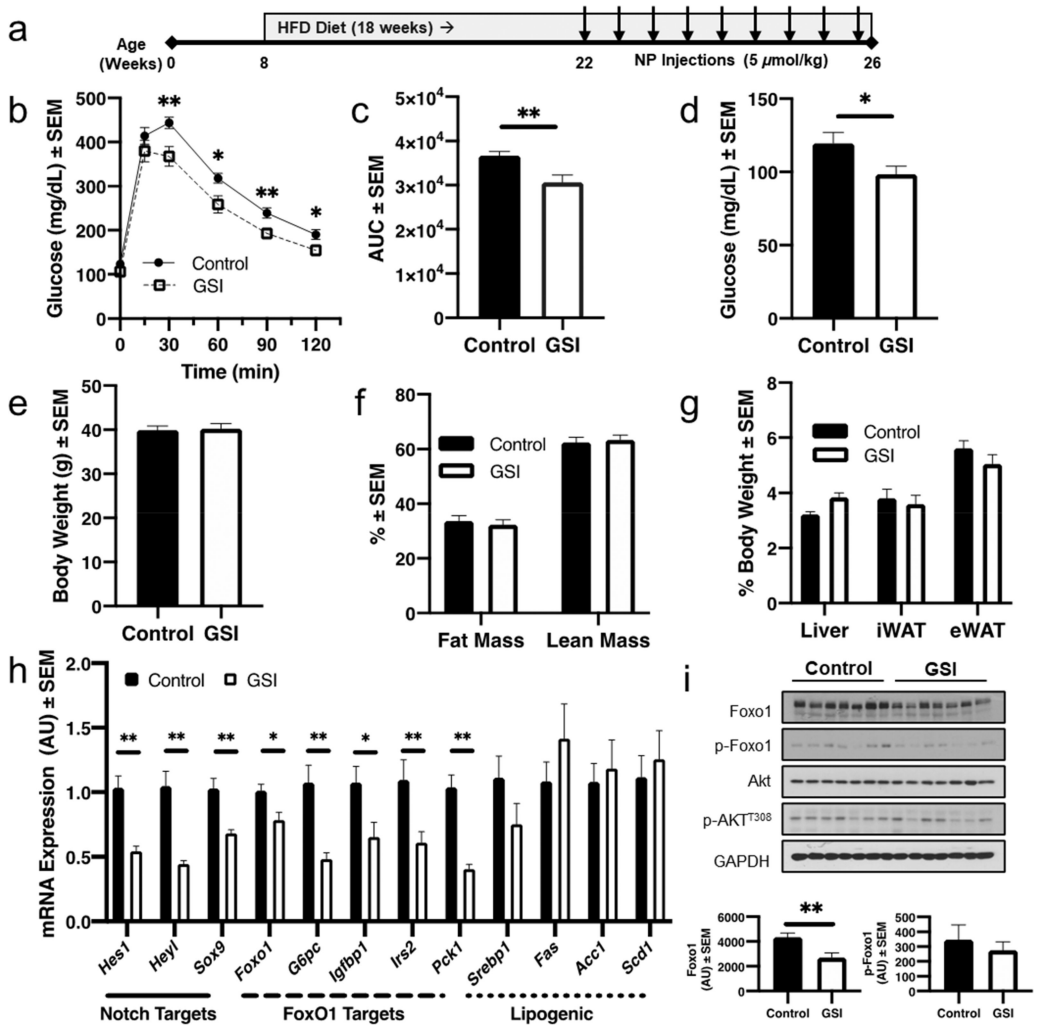

Figure 4.

GSI NP treatment improves HFD-induced glucose intolerance. (a) Experimental schematic. (b) GSI NPs reduce glucose excursion and (c) glucose area under the curve (AUC) after intraperitoneal glucose administration. (d) At sacrifice, GSI NPs reduced fasting blood glucose, without affecting (e) body weight, (f) body composition, or (g) liver and adipose tissue weights. (h) GSI NPs reduced Notch targets as well as expression of *Foxo1* and its target genes with (i) commensurately reduced liver Foxo1 and p-Foxo1^{S256} levels. *$p < 0.05$, **$p < 0.01$ as compared to control NP-treated mice, $n = 11–12$/group.

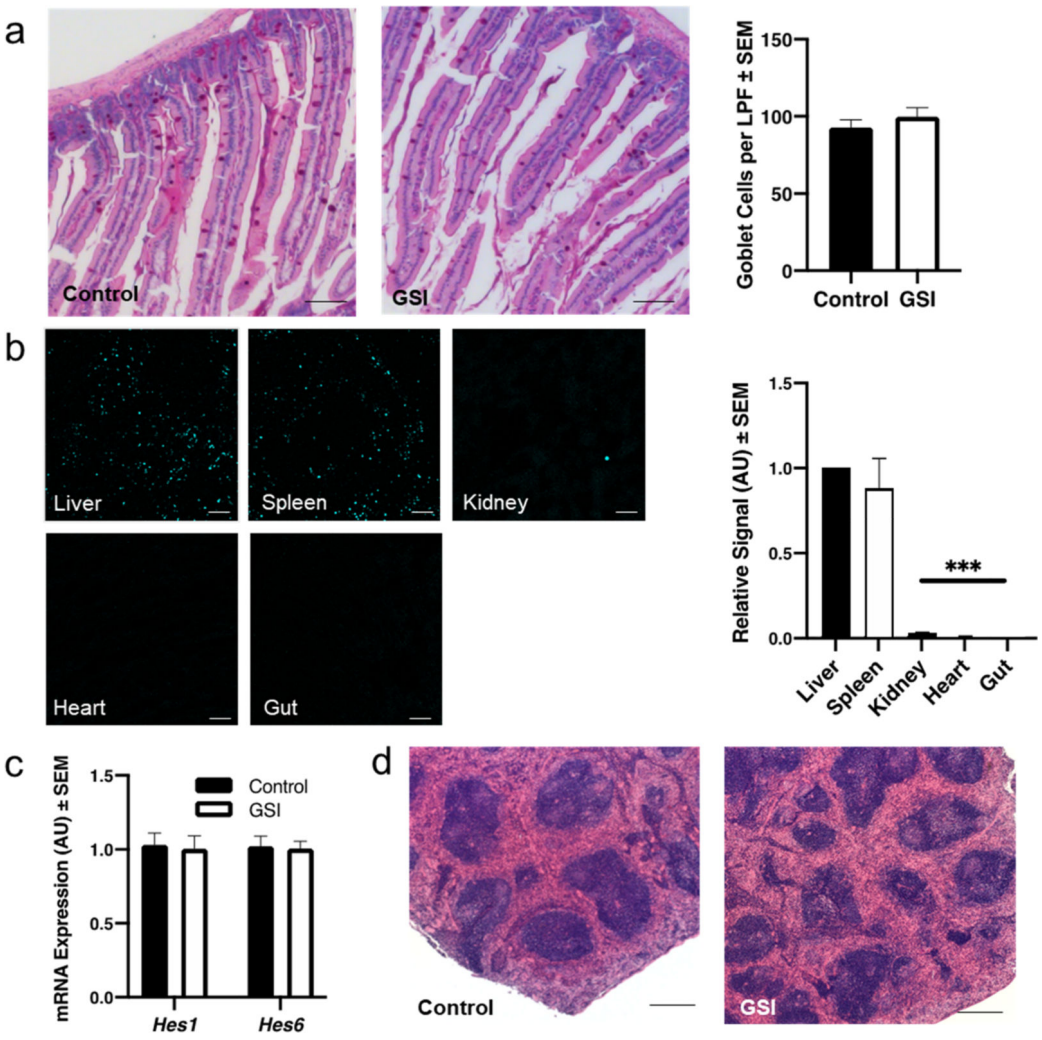

Figure 5.

GSI NPs do not induce intestinal or splenic toxicity. (a) Normal intestinal goblet cell number in GSI NP-treated mice by quantification of PAS+ cells (scale bar: 200 μm). (b) Representative confocal images of Cy5.5 signal in liver and extra-hepatic tissues taken from the same animal and quantification of signal relative to liver (scale bar: 200 μm). (c) Unchanged Notch target gene expression and (d) normal splenic architecture in GSI NP-treated mice (scale bar: 500 μm). ***$p < 0.001$ as compared to liver Cy5.5 signal, $n = 10$ (a) and 11–12/group.

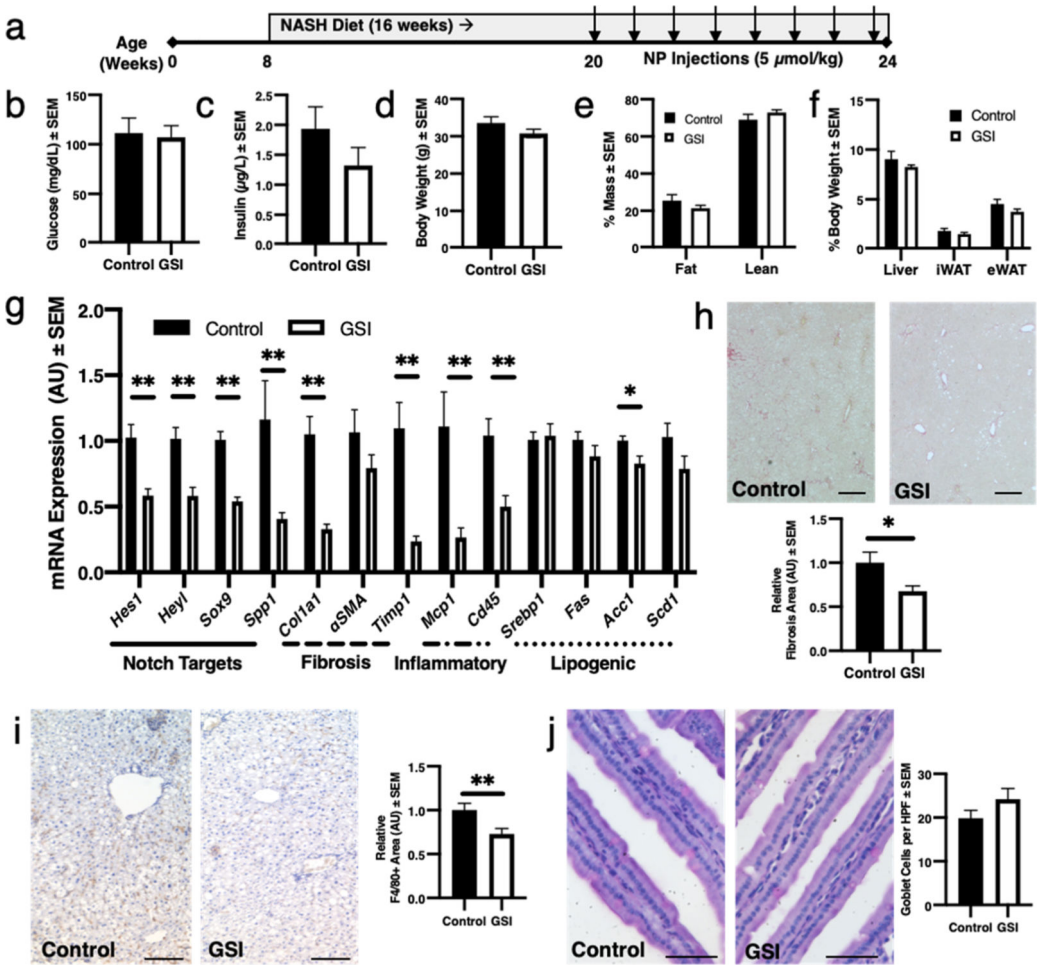

Figure 6.

GSI NPs ameliorate liver inflammation and fibrosis in NASH diet-fed mice. (a) Experimental schematic. (b–g) GSI NPs did not significantly affect (b) glucose, (c) insulin, (d) body weight, (e) body composition, or (f) liver and adipose tissue weights but (g) reduced Notch target and fibrogenic and inflammatory gene expression. (h) GSI NP-treated mice show reduced liver fibrosis by quantification of Picrosirius red (scale bar: 500 μm) and (i) F4/80+ staining (scale bar: 200 μm), without increase in (j) PAS+ intestinal goblet cells (scale bar: 50 μm). *$p < 0.05$, **$p < 0.01$ as compared to control NP-treated mice, $n = 6–9$/group.